tvst

Article

Scheimpflug-Based Analysis of the Reflectivity of the Cornea in Marfan Syndrome

Michèle Tack[1], Elke O. Kreps[1–3], Julie De Zaeytijd[1,2], and Alejandra Consejo[4,5]

[1] Department of Ophthalmology, Ghent University Hospital, Ghent, Belgium
[2] Faculty of Medical Sciences, Ghent University, Ghent, Belgium
[3] Faculty of Medical Sciences, Antwerp University, Antwerp, Belgium
[4] Department of Applied Physics, University of Zaragoza, Zaragoza, Spain
[5] Institute of Physical Chemistry, Polish Academy of Sciences, Warsaw, Poland

Correspondence: Alejandra Consejo, Department of Applied Physics, University of Zaragoza, Pedro Cerbuna 12, 50009 Zaragoza, Spain. e-mail: alejandra.consejo@unizar.es

Received: April 27, 2021
Accepted: June 29, 2021
Published: August 27, 2021

Keywords: marfan syndrome; corneal transparency; scheimpflug imaging; corneal reflectivity

Citation: Tack M, Kreps EO, De Zaeytijd J, Consejo A. Scheimpflug-based analysis of the reflectivity of the cornea in marfan syndrome. Transl Vis Sci Technol. 2021;10(9):34, https://doi.org/10.1167/tvst.10.9.34

Purpose: We sought to investigate corneal reflectivity in Marfan syndrome (MFS) on the basis of Scheimpflug light intensity distribution.

Methods: In a retrospective case-control analysis, the left eyes of 40 MFS patients and 40 age- and refraction-matched healthy controls were investigated. Patients with MFS meeting the Ghent II diagnostic criteria and with genetic confirmation of disease were included. Exclusion criteria were the following: coexisting corneal, conjunctival, or scleral pathology; use of medication known to affect corneal transparency; history of ocular surgery; and insufficient data. Scheimpflug tomography images were exported to analyze corneal transparency in different corneal layers and regions. Each corneal image was automatically segmented, after which the corresponding pixel intensities in the defined regions of interest were statistically modeled using a Weibull probability density function from which parameters α (transparency) and β (homogeneity) were derived.

Results: The cornea in MFS showed significantly higher light reflectivity (overall cornea, $\alpha = 71 \pm 17$ arbitrary units (a.u.)) than in the control group (overall cornea, $\alpha = 59 \pm 15$ a.u.) (*t* test, $P = 0.003$). The α parameter was significantly higher in MFS eyes in all examined layers and regions ($P < 0.05$), whereas the β parameter showed no statistical difference between MFS and controls ($P > 0.05$). The difference in α did not correlate with ocular biometric properties (corneal thickness and curvature) or ectopia lentis ($P > 0.05$).

Conclusions: The cornea in MFS shows significantly higher reflectivity than healthy controls with similar levels of homogeneity.

Translational Relevance: The proposed methodology detects corneal reflectivity changes in MFS not available from regular slit-lamp examination.

Introduction

Marfan syndrome (MFS) is an autosomal dominant connective tissue disorder caused by mutations in the *FBN1* gene on chromosome 15, which encodes the fibrillin-1 protein.[1] It is characterized by abnormalities of the musculoskeletal, cardiovascular, and ocular systems, linked to altered biomechanical properties in tissues containing elastic material.[1] Diagnosis is mainly clinical and based on the Ghent II Nosology, updated in 2010.[2] Ectopia lentis (major diagnostic criterion) and myopia >3 diopters (D) (minor criterion) are the only ocular features included in revised criteria, present in about 60% and 30% of MFS patients, respectively.[2–4] A spectrum of other ocular abnormalities has been recognized in MFS, including increased axial length, thinning and flattening of the cornea, iris abnormalities, and retinal detachment.[3–6] Fibrillin-1 polymers form the structural scaffold of extracellular, extensible microfibrils, which play a critical role in the strength and elasticity of ocular connective tissues, including

the ciliary zonules and the cornea.[7,8] Gene defects in *FBN1* lead to decreased and disordered incorporation of fibrillin into the connective tissue matrix.[9] Significant alterations to the corneal geometry have previously been demonstrated in MFS eyes: the cornea in MFS tends to be flatter and thinner and exhibits higher levels of corneal astigmatism as compared to healthy controls.[4,10,11] Relatively little is known about the pathogenesis of these corneal abnormalities.

In recent years, image processing techniques on the basis of statistical modeling of pixel intensity distribution have been used to gather information about the reflectivity properties of tissues in vivo, ranging from ultrasound scanning,[12] optical coherence tomography speckle,[13] and, most recently, the light intensity distribution of corneal Scheimpflug images.[14–17] Scheimpflug-based systems such as the Pentacam HR tomographer (Oculus Optikgeräte GmbH, Wetzlar, Germany) illuminate the cornea perpendicularly and image corneal cross-sections. Statistical analysis of the pixel intensity distribution in corneal Scheimpflug images has been shown to successfully discriminate mild keratoconus from control eyes[14,15] and quantify subclinical corneal changes associated with low-level hypoxia caused by scleral contact lens wear[16] and age-related corneal changes.[17] Microfibrils containing fibrillin-1 play an important role in the viscoelastic nature of the cornea, and therefore changes to this microfibrillar structure may result in a different pattern of light reflectivity by the cornea in MFS. The purpose of this study was to evaluate the reflectivity of the cornea in MFS with a custom-made automatic method on the basis of Scheimpflug imaging and to describe the correlation with other MFS-associated ocular signs.

Methods

Subjects and Data Collection

This retrospective comparative analysis was performed at the Department of Ophthalmology of Ghent University Hospital, Ghent, Belgium. Patients with a clinical diagnosis of MFS according to the Ghent II Nosology[2] and with genetic confirmation of disease (proven heterozygous *FBN1* mutation) were eligible for the study. The search engine of the electronic patient database (EyeFile, Aalter, Belgium) was used to identify MFS patients who visited the department between 2014 and 2019. Ophthalmic assessment included non-cycloplegic autorefraction (Nidek Ark-510A, Nidek Co., Ltd, Aichi, Japan), intraocular pressure (IOP) measurements via Goldmann applanation tonometry, dilated slit-lamp examination to assess lens subluxation, axial length measurement (IOLMaster 700; Carl Zeiss Meditec AG, Oberkochen, Germany) and Scheimpflug-based corneal tomography (Pentacam HR; Oculus, Wetzlar, Germany). In routine clinic, IOP measurements are performed after Pentacam imaging, to avoid interference of fluorescein staining of the tear film. Exclusion criteria were the following: insufficient quality of data ("OK" score on Pentacam HR was required), presence of any corneal, conjunctival, or scleral pathology, use of any medication known to affect corneal transparency, and history of ocular surgery. An age- and gender-matched control group, for whom the same exclusion criteria applied, was selected from the refractive clinic of the same hospital. The study was approved by the Ethics Committee of Ghent University Hospital and adhered to the tenets of the Declaration of Helsinki.

Data Analysis

To assess corneal transparency, the densitometry distribution analysis (DDA) was applied.[17] To apply the DDA, Scheimpflug images corresponding to the horizontal corneal meridian (a fixed size of 400 × 856 pixels) were exported for further analysis (i.e., 160 images in total = 80 subjects × 2 eyes/subject). The DDA data analysis procedure has been explained in detail elsewhere[15] and essentially consists of two stages: (i) corneal segmentation and (ii) statistical modeling of the pixel intensity distribution. Corneal segmentation allows for the selection of pixels in the image corresponding to the cornea, while separating them from the background and other ocular components. Subsequently, a region of interest (ROI) was extracted automatically for statistical modeling.

A fixed horizontal (lateral) ROI dimension of 600 pixels (approximately equivalent to 8 mm) was used for multilayer analysis, as indicated by Figure 1. To avoid undesired border effects (strong limbal/scleral reflections), the peripheral cornea (i.e., beyond 8 mm) was not included in the ROI, in agreement with previous literature.[16,17] As the epithelial border (Bowman's layer) is hardly visible on Scheimpflug images, it was decided to use an epithelial depth equivalent to 12% of the entire central corneal thickness previously delineated by corneal segmentation.[18] This epithelial layer was subtracted from the automatically delineated anterior corneal profile (Fig. 1, left), as in previous research.[16,17] The same procedure was applied to the posterior cornea, but the subtraction was done on the basis of the automatically delineated posterior corneal profile (Fig. 1, right). The central cornea, equivalent to the corneal stroma, was bordered by the ranges defined

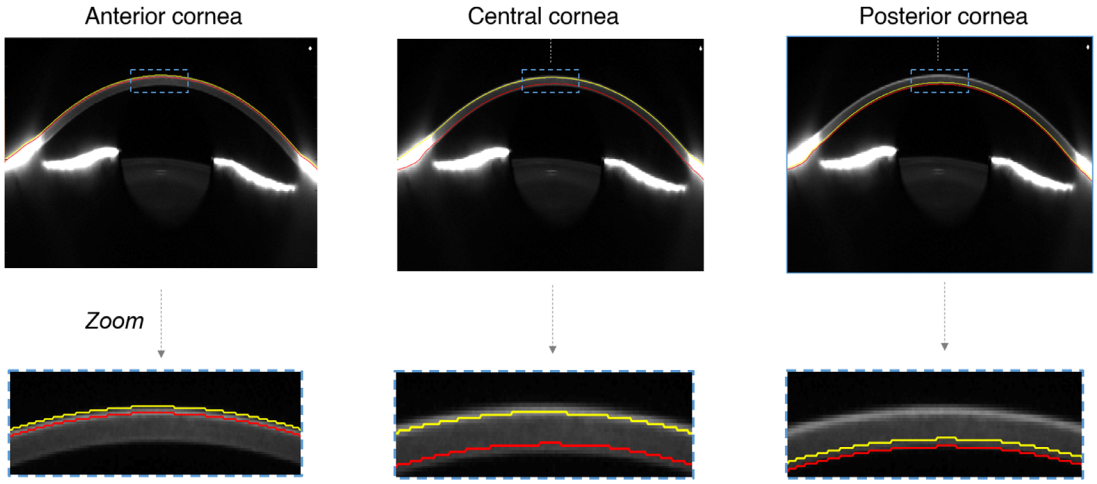

Figure 1. ROIs for depth analysis. *Yellow* and *red lines* demarcate anterior and posterior boundaries for each layer, respectively. The horizontal (lateral) ROI dimension was fixed to 600 pixels (approximately 8 mm). The vertical (axial) dimension of anterior, central and posterior corneal layers was demarcated depending on corneal thickness. *Blue dashed rectangles* zoom in on the corneal apex to illustrate the demarcation of the different layers.

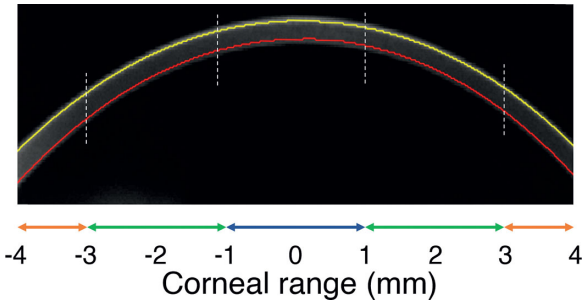

Figure 2. Sectors for regional analysis. *Yellow* and *red lines* demarcate anterior and posterior boundaries corresponding to the corneal stroma. The *blue arrow* delineates the central cornea (central 2 mm), *green arrows* mark the area from 2 to 6 mm and *orange arrows* highlight the area from 6 to 8 mm.

by the anterior and posterior cornea (Fig. 1, center). Consequently, the vertical (axial) dimension of the ROI depended on corneal thickness.

For regional (lateral) analysis, a fixed vertical (axial) dimension of the ROI was set for each subject corresponding to their central cornea (stroma). In this part of the analysis, image pixels corresponding to corneal epithelium were omitted from the ROI as they carried statistical information different from that of the stroma.[13] Five different ROIs were set, as indicated by Figure 2. The center of the cornea corresponded to the central 2 mm (blue double arrow in Fig. 2), mid cornea corresponded to the area from 2 to 6 mm (green double arrows in Fig. 2) and the peripheral cornea corresponded to the area from 6 to 8 mm (orange double arrows in Fig. 2). For statistical analysis, the nasal and temporal area were averaged within the corresponding section. Although ROIs differed in number of pixels, previous research has demonstrated, by means of bootstrap method, that the number of pixels in a given ROI does not affect the assessment of corneal transparency.[15] In other words, corneal thickness is not a confounding factor when applying the DDA method.

Furthermore, pixels corresponding to a given ROI were modeled using a distribution function, whereby the pixel intensity indicates how bright a given pixel is. The pixel intensity distribution of each ROI was approximated by the two-parameter distribution function that provides the best fit in the statistical analysis of the Scheimpflug light intensity distribution, namely the Weibull probability density function.[15] From this function, two parameters are extracted (α and β) which account for tissue transparency. In general, a change in the scale parameter (α) causes a shift along the pixel intensity axis (x-axis): an increase in α corresponds to an increase in pixel intensity (i.e., less transparent), and vice versa. A change in the shape parameter (β) affects the width of the pixel intensity distribution. The smaller β is, the greater the spread of the pixel intensity distribution of a given image, whereas a large β indicates greater similarity in pixel intensities within a given image or ROI.[16]

In addition to the assessment of corneal transparency in different corneal layers and regions, a moving ROI was applied across the cornea to investigate regional changes in corneal transparency in more detail, as explained elsewhere.[16] The moving ROI had a vertical (axial) dimension corresponding to the central cornea (stroma) as shown in the middle

image of Figure 1 and a horizontal (lateral) dimension of 11 pixels, covering the central 8 mm of the cornea (i.e., moving from −4 mm to 4 mm) in steps of 1 pixel. An 11 pixel-length moving ROI was chosen on the basis of previous research.[16] Finally, and exclusively for illustrative purposes, a subject from each group was randomly selected to compare corneal transparency of Marfan and control eyes at a glance. A square moving ROI of 3 × 3 pixels was applied to their corresponding corneal image, across their central 8 mm of the cornea, covering their full corneal thickness.

Statistical Analysis

The statistical analysis was performed using SPSS statistics software (SPSS Inc, Chicago, IL, USA). Normality of all sets of data was not rejected (Shapiro-Wilk test, $P > 0.05$). Independent *t*-test, F-test of equality of variances, and Pearson's correlation coefficient (r) were used to assess relationships within the continuous variables under investigation. The level of significance was set to 0.05. As corneal transparency values between right and left eyes of a subject are highly correlated,[19] eyes of the same subject were treated separately and not combined for statistical analysis. In

Table 1. Descriptive Parameters of the Left Eyes of MFS and Control Participants

	MFS	Controls	F-Test, *P* Value	*t*-Test, *P* Value
Age (years)			F(1,78) = 0.07, *P* = 0.79	0.94
	32.4 ± 10.3	32.5 ± 10.9		
	[20, 52]	[18, 58]		
Refractive error (D)			F(1,78) = 0.14, *P* = 0.71	0.54
	−2.10 ± 3.70	−2.50 ± 3.40		
	[−11.50, 10.50]	[−14.00, 3.00]		
K_{mean} (D)			F(1,78) = 2.29 , *P* = 0.13	<0.001*
	41.4 ± 1.7	43.2 ± 1.3		
	[37.2, 44.7]	[40.5, 46.9]		
CCT (µm)			F(1,78) = 0.02 , *P* = 0.88	<0.001*
	531 ± 31	560 ± 32		
	[468, 602]	[482, 627]		
PPI Avg			F(1,78) = 1.55, *P* = 0.22	0.97
	0.93 ± 0.18	0.93 ± 0.14		
	[0.51, 1.60]	[0.69, 1.34]		
Axial length (mm)			n/a	n/a
	24.2 ± 1.4	n/a		
	[21.3, 28.2]	n/a		
IOP (mm Hg)			F(1,78) = 0.94, *P* = 0.33	0.41
	13 ± 3	13 ± 3		
	[7, 20]	[8, 18]		
Pupil size (mm)			F(1,78) = 7.8, *P* = 0.007	n/a
	4.3 ± 1.8	3.8 ± 1.5		
	[2.0, 7.8]	[2.5, 8.2]		
ACD (mm)			F(1,78) = 0.05, *P* = 0.82	0.007*
	2.8 ± 0.4	3.1 ± 0.6		
	[1.3, 3.9]	[2.4, 3.7]		

The mean, standard deviation, and range in brackets are reported. The refractive error is listed as spherical equivalent, as obtained via non-cycloplegic autorefraction. The MFS and control groups were compared using the F-test and independent *t*-test. The condition of homogeneity of variance (homoscedasticity) was not met in pupil size, even following data transformation to a logarithmic scale and to reciprocals. Consequently, independent *t*-test and equivalent nonparametric tests could not be computed to compare pupil size between groups.

n/a, not available; K_{mean}, mean anterior keratometry; CCT, central corneal thickness; PPI Avg, Average Pachymetric Progression Index; IOP, intraocular pressure; ACD anterior chamber depth.

*Statistically significant result.

the Results section we report the findings for left eyes only except where otherwise stated.

Results

Participants

In this study, eyes of 40 MFS subjects and 40 healthy participants were included, resulting in data of 160 eyes in total. A subtle female predominance was found in both groups (22/40; 55%). The MFS and control participants were also matched in terms of age, refractive error (reported as spherical equivalent) and IOP. For descriptive purposes, the results of biometrical parameters are shown in Table 1 for MFS and control eyes. Of the included (left) eyes of MFS patients, 15 (37.5%) displayed no signs of lens subluxation (after dilated slit-lamp examination), 18 (45%) showed mild displacement of the crystalline lens (only visible following pupillary dilation), six (15%) had moderate lens subluxation (lens border visible in the pupillary aperture before dilation, and in one eye (2.5%) the lens had luxated into the vitreous.

Table 2. Group Mean Values ± Standard Deviation of α, and β for the Left Eye of Marfan and control participants

	MFS	Controls	*P* Value
Depth layers			
Anterior			
α	91 ± 19	77 ± 18	0.008*
β	2.5 ± 0.2	2.5 ± 0.2	0.90
Central			
α	73 ± 18	60 ± 15	0.003*
β	3.0 ± 0.3	3.1 ± 0.3	0.60
Posterior			
α	55 ± 15	45 ± 12	0.005*
β	4.3 ± 0.3	4.4 ± 0.3	0.27
Concentric regions			
0–2 mm			
α	70 ± 14	61 ± 12	0.007*
β	2.7 ± 0.3	2.8 ± 0.4	0.35
2–6 mm			
α	61 ± 13	52 ± 11	0.004*
β	2.6 ± 0.2	2.6 ± 0.2	0.85
6–8 mm			
α	82 ± 31	63 ± 24	0.006*
β	2.7 ± 0.5	2.8 ± 0.4	0.45
Overall			
α	71 ± 17	59 ± 15	0.003*
β	2.7 ± 0.3	2.7 ± 0.3	0.51

α, β are expressed in arbitrary units. Values of both groups were compared using the independent t-test.

*Statistically significant result.

Corneal Light Reflectivity

Findings pertaining to the Scheimpflug light distribution analysis are listed in Table 2. Overall, the cornea in MFS eyes was found to be more reflective (total cornea, $\alpha = 71 \pm 17$ arbitrary units) than the cornea in controls (total cornea, $\alpha = 59 \pm 15$ arbitrary units). Of the two available parameters to account for corneal reflectivity (α and β), α proved to be the most discriminant parameter, whereas β showed no significantly different result for any depth or region examined. Consequently, additional focus was given to the α parameter and its specific properties. The largest difference between MFS and control participants in terms of reflectivity was found in the nasal area, as indicated by Figure 3. For illustrative purposes, Figure 4 shows the detailed distribution of the α and β parameter in the central 8 mm of the cornea for a randomly selected MFS and a matched control participant.

Correlation of Corneal Reflectivity With Biometrical Parameters

As Table 3 indicates, corneal reflectivity was found to be well correlated with age for both MFS ($r(\alpha) = 0.54$, $P < 0.001$; $r(\beta) = 0.50$, $P < 0.001$) and control participants ($r(\alpha) = 0.47$, $P < 0.001$; $r(\beta) = 0.49$, $P < 0.001$)). In addition, corneal reflectivity was found to be moderately correlated with anterior chamber depth (ACD) but only for control participants ($r(\alpha) = -0.35$, $P = 0.012$; $r(\beta) = -0.40$, $P = 0.006$). No other significant correlations were found between α and β parameters and biometrical parameters. No correlation was found between the level of lens subluxation (no/mild/moderate/luxation) and corneal reflectivity (all pairwise comparisons, independent *t*-test, $P > 0.05$).

Discussion

The present study reports on the in vivo assessment of the light reflectivity of the cornea in MFS eyes. The Scheimpflug-based analysis used in this study generates quantitative values of two parameters, whereby the α parameter relates to pixel intensity and the β parameter represents the uniformity of pixel intensities in an examined region.[16] A distinct pattern of changes in reflectivity was identified in MFS corneas.

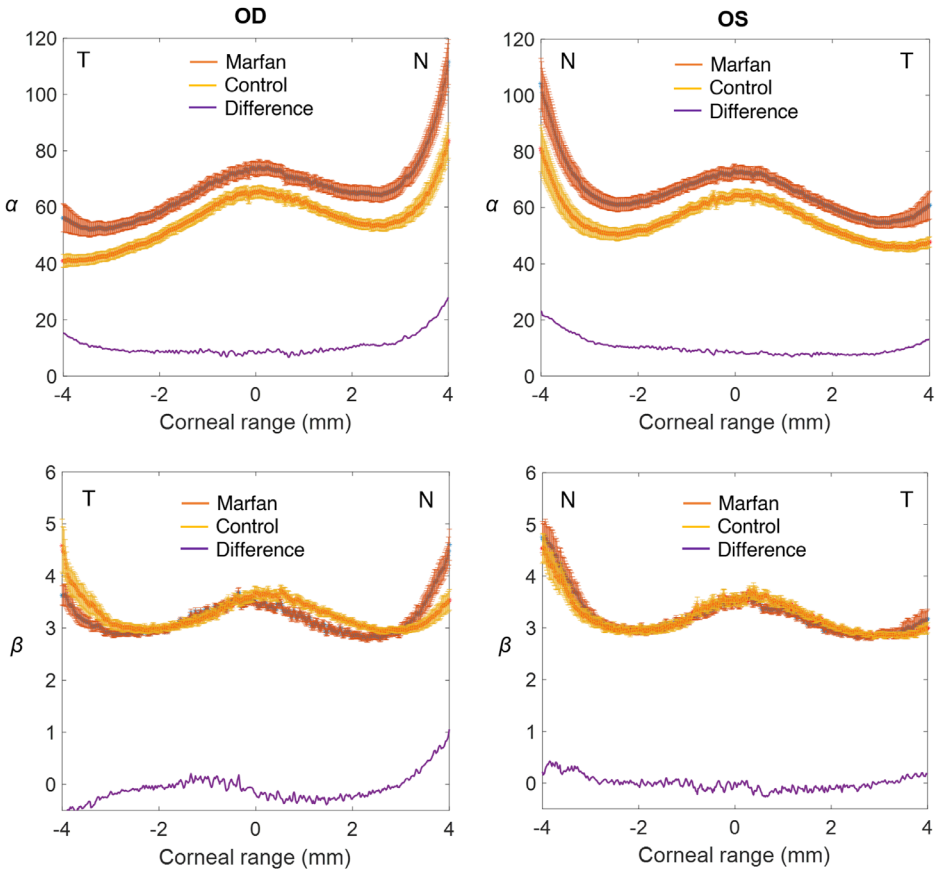

Figure 3. Mean value of the α parameter (*top*) and β parameter (*bottom*) for the stroma of MFS (in *orange*) and control eyes (in *yellow*) and the difference between them (in *purple*) for the right (OD) and left eye (OS) of the central-8-mm cornea of the participants. *Error bars* indicate the standard error. N, nasal; T, temporal.

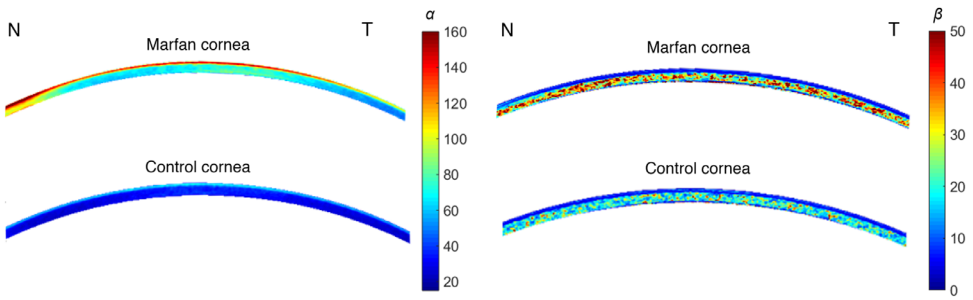

Figure 4. Distribution of α (*left*) and β (*right*) parameter for the central 8 mm of the left cornea of an MFS participant (male, 49 years old) and a control participant (female, 39 years old). The *color bar* is expressed in arbitrary units. N, nasal; T, temporal.

Significantly higher values of α were detected in MFS as compared to control corneas. In contrast, no difference in the β parameter was found. These findings were seen in all examined layers and regions of the cornea in a rather consistent and uniform manner (as displayed in Fig. 3). Hence, the MFS cornea reflects more light than a normal cornea (i.e., is less transparent), but with similar levels of homogeneity. The largest difference in α parameter was seen in the nasal area, but the origin of this trend remains unclear.

Corneal light transmission is governed by a highly organized framework of cellular and extracellular components.[20] When divided by layer, the anterior layer showed the highest reflectivity in both MFS and control eyes, which aligns with prior studies on the levels of backscattered light in the normal cornea.[19]

Table 3. Pearson Correlation Between α Parameter and Different Biometrical Parameters

	MFS	Controls
Age (years)	0.54 ($P < 0.001$)*	0.47 ($P < 0.001$)*
Refractive error (D)	0.06 ($P = 0.37$)	0.15 ($P = 0.18$)
K_{mean} (D)	−0.17 ($P = 0.15$)	−0.04 ($P = 0.39$)
CCT (µm)	−0.24 ($P = 0.07$)	0.00 ($P = 0.50$)
PPI Average	0.13 ($P = 0.21$)	0.40 ($P = 0.16$)
Axial length (mm)	0.05 ($P = 0.38$)	N/A
IOP (mm Hg)	0.23 ($P = 0.07$)	−0.23 ($P = 0.07$)
Pupil size (mm)	−0.16 ($P = 0.16$)	−0.09 ($P = 0.28$)
ACD (mm)	−0.24 ($P = 0.07$)	−0.35 ($P = 0.012$)*

n/a, not available; K_{mean}, mean anterior keratometry; CCT, central corneal thickness; PPI, Average Pachymetry progression index; IOP, intraocular pressure; ACD anterior chamber depth.

*Statistically significant result.

Fibrillin-1 has been immunolocalized to the basement membrane zone of the corneal epithelium, which may account for the detected differences in transparency between MFS and normal corneas in the anterior layer.[8]

Stromal reflectivity is chiefly dependent on the narrow, uniform diameter of collagen I fibrils and the regularity of the spacing between these collagen fibrils, which itself is regulated by the interaction of collagen with interfibrillar proteoglycans.[20] In recent years, advanced imaging techniques have led to novel insights into the presence and role of fibrillin-1 containing microfibrils within the corneal stroma.[21] In contrast with microfibrils in the sclera, which carry an elastin core, the stroma of a normal human cornea contains a network of elastin-free, fibrillin-1-containing microfibrils, most abundant in the posterior stroma and becoming progressively less present anteriorly.[22] In *FBN 1*$^{+/-}$ mouse corneas, significantly reduced amounts of fibrillin-1-containing microfibrils have been detected, as well as microfibril disorganization compared to controls, both at the adult and late embryonic stage.[22,23] The lens capsule in human MFS patients has similarly showed both quantitative and qualitative changes, with irregular and fragmented bundles evident upon histologic analysis.[24] In adult *FBN 1*$^{+/-}$ mouse corneas, the interfibrillar spacing of collagen fibrils has been shown to be increased, despite the reduced corneal thickness, which indicates a lower number of collagen lamellae in the adult *FBN 1*$^{+/-}$ corneas compared to wild-type mice.[22,23] The exact cause of the altered collagen organization in MFS remains unknown but may relate to the decreased decorin levels or the higher TGF-β activity detected in MFS corneas.[23] The increased stromal reflectivity detected in MFS eyes in this study may reflect the altered collagen architecture and consequently, the optical properties of the stroma. In vivo confocal microscopy (IVCM) of the cornea of MFS patients have also demonstrated increased backscattering of light at the level of the stroma because of a highly reflective extracellular matrix of the stroma.[10,25]

Significantly higher α parameter values were also detected in the posterior cornea in MFS eyes as compared to controls in this study. Although no fibrillin staining has been demonstrated in Descemet membrane or the corneal endothelium in histopathologic assessment of healthy eyes,[8] IVCM has detected changes to the endothelium in MFS corneas.[10,25] Thin, brightly reflective particles, not present in the control group, were found in the corneal endothelium of MFS corneas, reminiscent of the "black spots" detected in the center of endothelial cells in MFS patients in an older specular microscopy study.[25,26] The exact nature of these endothelial findings in MFS eyes remains elusive.

The second aim of this study was to examine the correlation between characteristics of corneal light reflectivity and recognized MFS-associated ocular signs. The MFS cornea in this study was found to be flatter and thinner as compared to controls, which aligns with prior research, although conflicting data regarding central corneal thickness in MFS are found in literature.[3–5,11] Previous studies on patients with MFS showed an average axial length of 24.0–25.0 mm,[3–5] as detected in this cohort. None of the included ocular parameters, including ectopia lentis, were significantly correlated with the α parameter in MFS. An age-related increase in corneal reflectivity was detected in both the MFS and control group, the latter aligning with previous research.[17,19] It confirms the need for age-matched groups when comparing corneal

reflectivity, as was done in this study. In control eyes, corneal reflectivity was also moderately correlated with ACD. The ACD is known to correlate strongly with age (decrease of ACD with age).[27] This finding may therefore be a confounder effect rather than an actual correlation between variables, particularly as it was only observed in the control group and age showed a much stronger correlation ($P < 0.001$) than ACD.

Changes to ocular biometric characteristics, including corneal thinning and flattening, are typically more pronounced in MFS eyes with ectopia lentis, whereas eyes without overt lens subluxation remain diagnostically challenging.[4,5,10] Similarly, corneal macroscopic biomechanical properties, as studied with the Ocular Response Analyzer (Reichert, Inc), were only found to be significantly altered in MFS eyes with ectopia lentis[28] and MFS patients with high systemic score points.[29] The pattern of parameters α and β may aid in diagnosing MFS eyes in the absence of overt clinical signs such as ectopia lentis, particularly in conjunction with macroscopic corneal thickness and curvature measurements retrieved from the same Scheimpflug device. Given the known correlation of α with age, age-adjusted formulas will be required to investigate further the role of these parameters within a diagnostic context.

Corneal backscatter has been quantified in a number of ways, including backscatter measurements on IVCM and corneal densitometry.[19,30] For diagnostic purposes, IVCM has major drawbacks. It requires a specially trained physician to operate the microscope and the repeatability of backscatter measurements is known to be very low.[30] Additionally, IVCM is not widely available whereas Scheimpflug devices are widespread across corneal clinics. The Scheimpflug-based Ocular Pentacam includes a densitometry (DS) analysis as an add-on to the standard software, which offers data on the amount of backscattered light in different regions of the cornea.[19] The DS analysis is platform-dependent (only available on the Pentacam HR) and is limited to providing a mean value of the amount of backscattered light, rather than the two separate parameters provided by the DDA, based on Scheimpflug light distribution analysis, used in this study. Additionally, the DDA method here used has already shown to work with Scheimpflug devices other than Pentacam HR,[17] which highlights the platform independency of the method. The analysis of α and β was performed on a single corneal meridian (horizontal meridian), whereas the Pentacam HR module uses 25 meridians that are interpolated to reconstruct a complete DS map. Although this could be seen as a limitation of the current study, the ability to extract corneal reflectivity measurements comparable with those from DS based on a single image has been already proven.[17] In a previous work, α and β (extracted from a single meridian) were found to be well correlated with densitometry (calculated from 25 meridians), especially α (overall cornea; $r = 0.89$, $P < 0.001$).[17] One of the main limitations of this study is the lack of axial length data in the control group. Findings reported in this study should be confirmed in a larger cohort. Previous studies on the Scheimpflug light intensity distribution included normal and keratoconus eyes, in which eyes with mild keratoconus showed a distinctly different pattern as described in MFS corneas in this study.[14,15] It would be of particular interest to compare findings in MFS eyes with other hereditary connective tissue diseases, such as Ehlers-Danlos syndrome to investigate the disease-specific nature of findings reported in this study.

In summary, significant changes to the corneal light intensity distribution were detected in MFS eyes compared to age-matched controls. In all corneal layers and regions examined, higher levels of light backscatter were detected in MFS-affected corneas. This increase in light reflectivity was found to be independent of other MFS-associated ocular characteristics.

Acknowledgments

Supported by the National Science Centre (Poland) under the OPUS 19 funding scheme; project no. 2020/37/B/ST7/00559.

Disclosure: **M. Tack,** None; **E.O. Kreps,** None; **J. De Zaeytijd,** None; **A. Consejo,** None

References

1. Kumar A, Agarwal S. Marfan syndrome: An eyesight of syndrome. *Meta Gene.* 2014;2:96–105.
2. Loeys BL, Dietz HC, Braverman AC, et al. The revised Ghent nosology for the Marfan syndrome. *J Med Genet*. 2010;47(7):476–485.
3. Kinori M, Wehrli S, Kassem IS, et al. Biometry Characteristics in Adults and Children With Marfan Syndrome: From the Marfan Eye Consortium of Chicago. *Am J Ophthalmol*. 2017;177:144–149.
4. Maumenee IH. The eye in the Marfan syndrome. *Trans Am Ophthalmol Soc*. 1981;79:684–733.
5. Nemet AY, Assia EI, Apple DJ, Barequet IS. Current concepts of ocular manifestations in Marfan syndrome. *Surv Ophthalmol*. 2006;51(6):561–575.

6. Gehle P, Goergen B, Pilger D, et al. Biometric and structural ocular manifestations of Marfan syndrome. *PLoS One*. 2017;12(9):e0183370.
7. Verstraeten A, Alaerts M, Van Laer L, Loeys B. Marfan syndrome and related disorders: 25 years of gene discovery. *Hum Mutat*. 2016;37(6):524–531.
8. Wheatley HM, Traboulsi EI, Flowers BE, et al. Immunohistochemical localization of fibrillin in human ocular tissues; relevance to the Marfan syndrome. *Arch Ophthalmol*. 1995;113(1):103–109.
9. Hollister DW, Godfrey M, Sakai LY, Pyeritz RE. Immunohistologic abnormalities of the microfibrillar-fiber system in the Marfan syndrome. *N Engl J Med.* 1990;323(3):152–159.
10. Sultan G, Baudouin C, Auzerie O, et al. Cornea in Marfan disease: Orbscan and in vivo confocal microscopy analysis. *Invest Ophthalmol Vis Sci.* 2002;43:1757–1764.
11. Heur M, Costin B, Crowe S, et al. The value of keratometry and central corneal thickness measurements in the clinical diagnosis of Marfan syndrome. *Am J Ophthalmol*. 2008;145:997–1001.
12. Tunis AS, Czarnota GJ, Giles A, et al. Monitoring structural changes in cells with high-frequency ultrasound signal statistics. *Ultrasound Med Biol*. 2005;31:1041–1049.
13. Jesus DA, Iskander DR. Assessment of corneal properties based on statistical modeling of OCT speckle. *Biomed Opt Express*. 2016;8:162–176.
14. Consejo A, Glawdecka K, Karnowski K, et al. Corneal properties of keratoconus based on Scheimpflug light intensity distribution. *Invest Ophthalmol Vis Sci.* 2019;60:3197–3203.
15. Consejo A, Solarski J, Karnowski K, et al. Keratoconus detection based on a single Scheimpflug image. *Transl Vis Sci Technol*. 2020;9(7):36.
16. Consejo A, Alonso-Caneiro D, Wojtkowski M, Vincent SJ. Corneal tissue properties following scleral lens wear using Scheimpflug imaging. *Ophthalmic Physiol Opt.* 2020;40:595–606.
17. Consejo A, Jiménez-García M, Rozema JJ. Age-related corneal transparency changes evaluated with an alternative method to corneal densitometry. *Cornea*. 2020;40:215–222.
18. Li HF, Petroll WM, Møller-Pedersen T, et al. Epithelial and corneal thickness measurements by in vivo confocal microscopy through focusing (CMTF). *Curr Eye Res.* 1997;16:214–221.
19. Ni Dhubhghaill S, Rozema JJ, Jongenelen S, et al. Normative values for corneal densitometry analysis by Scheimpflug optical assessment. *Invest Ophthalmol Vis Sci.* 2014;55:162–168.
20. Meek KM, Fullwood NJ. Corneal and scleral collagens—a microscopist's perspective. *Micron*. 2001;32:261–272.
21. Lewis PN, White TL, Young RD, et al. Three-dimensional arrangement of elastic fibers in the human corneal stroma. *Exp Eye Res*. 2016;146:43–53.
22. White TL, Lewis P, Hayes S, et al. The Structural Role of Elastic Fibers in the Cornea Investigated Using a Mouse Model for Marfan Syndrome. *Invest Ophthalmol Vis Sci.* 2017;58:2106–2116.
23. Feneck EM, Souza RB, Lewis PN, Hayes S, Pereira LV, Meek KM. Developmental abnormalities in the cornea of a mouse model for Marfan syndrome. *Exp Eye Res*. 2020;194:108001.
24. Traboulsi EI, Whittum-Hudson JA, Mir S, Maumenee IH. Microfibril abnormalities of the lens capsule in patients with Marfan syndrome and ectopia lentis. *Ophthal Genet*. 2000;21:9–15.
25. Iordanidou V, Sultan G, Boileau C, et al. Marfan Study Group. In vivo corneal confocal microscopy in Marfan syndrome. *Cornea*. 2007;26:787–792.
26. Setälä K, Ruusuvaara P, Karjalainen K. Corneal endothelium in Marfan syndrome. A clinical and specular microscopic study. *Acta Ophthalmol (Copenh)*. 1988;66:334–40.
27. Phu J, Tong J, Zangerl B, Le JL, Kalloniatis M. Cluster analysis reveals patterns of age-related change in anterior chamber depth for gender and ethnicity: clinical implications. *Ophthalmic Physiol Opt*. 2020;40:632–649.
28. Kara N, Bozkurt E, Baz O, et al. Corneal biomechanical properties and intraocular pressure measurement in Marfan patients. *J Cataract Refract Surg*. 2012;38:309–314.
29. Scheibenberger D, Frings A, Steinberg J, et al. Ocular manifestation in Marfan syndrome: corneal biomechanical properties relate to increased systemic score points. *Graefes Arch Clin Exp Ophthalmol*. 2018;256:1159–1163.
30. Hillenaar T, Cals RH, Eilers PH, et al. Normative database for corneal backscatter analysis by in vivo confocal microscopy. *Invest Ophthalmol Vis Sci*. 2011;52(10):7274–7281.